Journal of Applied Fluid Mechanics, Vol. 10, No. 5, pp. 1355-1362, 2017.
Available online at www.jafmonline.net, ISSN 1735-3572, EISSN 1735-3645.
DOI: 10.18869/acadpub.jafm.73.242.27698

Hydrodynamic Modelling of Coal-Biomass Mixture in a Bubbling Fluidized Bed Reactor

M. Verma[1, 2], C. Loha[1 †], A. N. Sinha[2], M. Kumar[3], A. Saikia[3], P. K. Chatterjee[1]

[1]*Energy Research and Technology, CSIR-Central Mechanical Engineering Research Institute, Durgapur-713209, India*
[2]*Department of Mechanical Engineering, National Institute of Technology Patna, Patna-800005, India*
[3] *Department of Mechanical Engineering, Indian Institute of Technology Guwahati, Guwahati-781039, Assam, India*

†*Corresponding author Email: chanchal.loha@gmail.com*

(Received February 17, 2017; accepted May 14, 2017)

ABSTRACT

Biomass is a renewable and sustainable energy source. Co-firing of biomass with coal will increase the renewable energy share by decreasing the coal consumption. In the present paper, hydrodynamic behaviour of coal and biomass mixture is investigated in a fluidized bed reactor. A Computational Fluid Dynamic (CFD) model is developed and the hydrodynamic behaviour of gas and solid is investigated in detail. The CFD model is based on Eulerian-Eulerian multiphase modelling approach where the solid phase properties are obtained by applying the Kinetic Theory of Granular Flow (KTGF). Six different weight percentages of coal and biomass (100:0, 95:5, 90:10, 80:20, 70:30 and 50:50) are used for the present study. The hydrodynamic behaviour is analyzed in terms of the important hydrodynamic parameters like bed pressure drop, bed expansion ratio, particle volume fraction distribution and velocity distribution. The numerical model is also validated by comparing some of the numerical results with our own experimental data generated in a laboratory scale bubbling fluidized bed reactor.

Keywords: Hydrodynamics; Fluidized bed; Biomass; Coal; CFD modelling.

NOMENCLATURE

d	particle diameter
e_{ss}	coefficient of restitution
$\vec{g}$	coefficient of restitution Acceleration due to gravity
$g_{o,ss}$	radial distribution function
g	gas
I	unit tensor
p	pressure
Re	Reynolds number
s	solid
t	time
$\vec{v}$	velocity vector
ρ	density
μ	shear viscosity
λ	bulk viscosity
Θ	granular temperature
ϕ	specularity coefficient
φ	exchange of fluctuating energy
k	diffusion coefficient
Υ	collsional dissipation of energy

Subscripts

α	volume fraction
$\bar{\bar{\tau}}$	shear stress tensor

1. INTRODUCTION

India is blessed with substantial biomass resources. The annual biomass production in India is estimated as 200 million tons. This is equivalent to 20 GW power. In addition, biomass obtained from agro-residues and woody bio-residues could add another 100-300 million tons (Buragohani *et al*. 2010). The co-firing of biomass to the existing coal fired power plants is a promising technology to increase the share of biomass for energy generation. There are a number of advantages of co-firing of biomass in coal based power plants. Co-firing lowers the huge capital costs involved in the dedicated biomass fired power plants by little modifications in existing coal fired power plants. Different biomass residues and energy crops could be used in coal fired power plants which

can diversify the fuel portfolio in coal fired plants. It will reduce CO_2 emission by saving the fossil fuels. It will also reduce the emission of NOx and SOx because nitrogen and sulphur content in most of the biomass materials are less (Verma *et al*., 2017).

In order to investigate the co-firing performance of coal and biomass mixture, a laboratory scale bubbling fluidized bed reactor is developed at CSIR-CMERI, Durgapur, India. However, before studying the actual co-firing performance, the basic gas-solid hydrodynamics of coal and biomass mixture is required to be investigated thoroughly. Most of the hydrodynamic studied on fluidized bed system available in open literature deal with mono-dispersed particles (Witta *et al*. 1998; Zimmermann *et al*. 2005; Deen *et al*. 2006; Yu *et al*. 2007; Zhu *et al*. 2008; Armstrong *et al*. 2010; Wang *et al*. 2010; Sau *et al*. 2011; Loha *et al*. 2012; Cloete *et al*. 2013). There are very few studies available on the fluidized bed hydrodynamics of mixture of particles having different diameters and/or densities. Gao *et al*. (2008) studied the flow behaviour of a gas–solid fluidized bed experimentally and numerically with fine FCC catalyst particles and coarse millet particles. The results showed that the smaller particles try to accumulate near the bed surface while the larger particles try to accumulate at the bottom in turbulent fluidized bed. The segregation efficiency increased with increasing gas velocity and mean residence time of particles, but decreased with increasing the small particle concentration. Busciglio *et al*. (2012) studied the hydrodynamic behaviour of binary mixtures of corundum particles and glass particles in bubbling fluidized bed experimentally. They measured bubble diameter, number of bubbles and their rising velocity and also described the bubbling dynamics in different operating conditions. Zhang *et al*. (2012) studied the hydrodynamic of binary mixture (tobacco stem and cation exchange resin) where the superficial gas velocity was operated in the range of two to five times of the minimum fluidization velocity. It was suggested that for satisfactory operation of bubbling fluidized bed the mass fraction of tobacco stem should be less than 7%. But, it can also be operated with higher tobacco stem by introducing jetting gases. Hydrodynamic behaviour of ground walnut shells and glass beads mixture was studied experimentally and numerically in a fluidized bed by Bai *et al*. (2013). Effects of mixture composition, particle size and superficial gas velocity were investigated on the mixing and segregation behaviour. It was observed that superficial gas velocity had a significant influence on particle segregation. Sharma *et al*. (2014) studied the hydrodynamic behavior of a mixture of biomass and biochar inside a bubbling fluidized bed reactor using Computational Fluid Dynamics (CFD) simulation. Effects of superficial gas velocity, biomass density and particle size of biomass were investigated on the hydrodynamic performance of biomass–biochar mixture. It was found that the size of bubbles increased as the superficial gas velocity increased and a better mixing of biomass and biochar was achieved. It was also observed that the density of biomass had a significant impact on the distribution of biomass in the biochar bed. Chen *et al*. (2015) studied the hydrodynamic behaviour of titanium slag and carbon particles in a bubbling fluidized bed system. They showed that the gas velocity significantly influenced bubble size. At low gas velocity, dominant bubbles enlarged with increasing the superficial gas velocity. On the other hand, at high gas velocity, the number of small bubbles increased with increasing the superficial gas velocity.

Despite some studies on hydrodynamic of binary mixture, studies on the hydrodynamic behaviour of coal and biomass mixture are limited in open literature and further study is required. In this paper, a detail numerical study on hydrodynamic behaviour of coal and biomass mixture in a bubbling fluidized bed reactor is presented. Eulerian-Eulerian Computational Fluid Dynamic (CFD) model is used for the simulation. Coal and biomass particles are modelled as two different solid phases with different properties. Six different weight percentages of coal and biomass (100:0, 95:5, 90:10, 80:20, 70:30 and 50:50) are used for the present study. The pressure drop across the bed, bed expansion ratio, particle volume fraction distribution and velocity distribution are investigated in detail. Some of the numerical results are also compared with our own experimental results obtained from the laboratory scale bubbling fluidized bed reactor.

2. EXPERIMENTAL INVESTIGATION

2.1 Experimental Setup

The experimental investigation is carried out in a laboratory scale bubbling fluidized bed reactor installed at Energy Research and Technology Group of CSIR-Central Mechanical Engineering Research Institute, Durgapur, India. The schematic diagram of experimental test set-up is shown in Fig. 1. The reactor is three dimensional and cylindrical in shape. Internal diameter of the reactor is 80 mm in the bed zone and 125 mm in the freeboard zone. Total height of the reactor is 1000 mm. The feeding of coal is done through a rotary feeder while feeding of biomass is done through a screw feeder. Air from a compressor is used as fluidizing medium and it is introduced from the bottom through the distributor plate. Air flow rate is measured using a rotameter and the flow rate is controlled by using gate valve. Pressure taps are provided to measure the pressure drop across the bed. U-tube water manometers are connected to the pressure taps for measuring the pressure. A cyclone separator is provided to arrest fine particles entrained by air.

2.2 Experimental Procedure

Before starting the experiment, coal and biomass samples are sieved using a series of sieves of different mesh sizes. Sawdust is used as the biomass material here. The mean particle diameter of coal and biomass are 750 μm and 600 μm respectively. Density of coal and biomass are 1198 kg/m^3 and 600 kg/m^3 respectively. Six different weight percentages of coal and biomass are used like 100:0, 95:5, 90:10, 80:20, 70:30 and 50:50. Coal and biomass are fed to the

reactor separately. Coal and biomass particles are fluidized with different flow rate of air. For each coal and biomass percentage, pressure drop and bed expansion ratios are measured with different flow rate of air. All experiments are carried out five times and average values are taken.

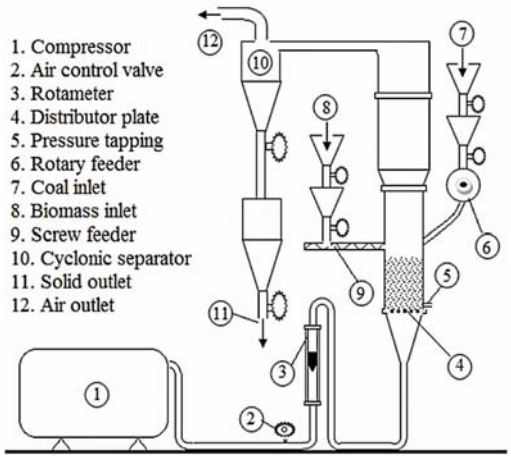

Fig. 1. Schematic diagram of the laboratory scale bubbling fluidized bed reactor.

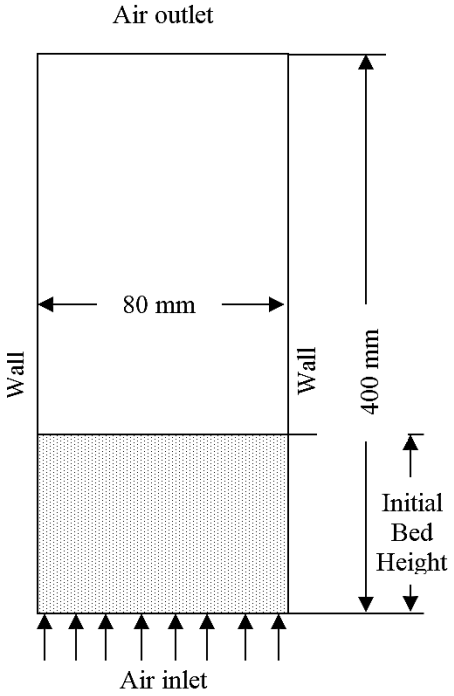

Fig. 2. Computational geometry.

3. SIMULATION AND MODELLING

3.1 Computational Geometry

The computational geometry refers to a 2D bubbling fluidized bed reactor of width 80 mm and height 400 mm as shown in Fig. 2. In order to reduce the computational cost, the freeboard region is not considered. Initially, particles are filled inside the reactor upto a bed height as per the experiments. Air is applied with a uniform velocity throughout the bottom inlet. The top of the reactor is open to the atmosphere.

3.2 Mathematical Equations

The Eulerian-Eulerian CFD model is used for the present simulation. In the Eulerian-Eulerian model, gas and solid phases are treated mathematically as interpenetrating continuum and their conservation equations are solved separately (Loha *et al.* 2012). Coupling between gas and solid phases is attained through the inter-phase forces like drag force, lift force and virtual mass force. In dense fluidized bed system, forces other than the drag force are usually not considered because of their negligible values. The mathematical equations used in Eulerian-Eulerian multiphase flow model are as follows:-

Continuity equations:

$$\frac{\partial}{\partial t}\left(\alpha_g \rho_g\right) + \nabla.\left(\alpha_g \rho_g \vec{v}_g\right) = 0 \quad (1)$$

$$\frac{\partial}{\partial t}\left(\alpha_s \rho_s\right) + \nabla.\left(\alpha_s \rho_s \vec{v}_s\right) = 0 \quad (2)$$

Momentum equations:

$$\frac{\partial}{\partial t}\left(\alpha_g \rho_g \vec{v}_g\right) + \nabla.\left(\alpha_g \rho_g \vec{v}_g \vec{v}_g\right) = -\alpha_g.\nabla p + \nabla.\bar{\bar{\tau}}_g + \alpha_g \rho_g \vec{g} + K\left(\vec{v}_s - \vec{v}_g\right) \quad (3)$$

$$\frac{\partial}{\partial t}\left(\alpha_g \rho_g \vec{v}_g\right) + \nabla.\left(\alpha_g \rho_g \vec{v}_g \vec{v}_g\right) = -\alpha_g.\nabla p + \nabla.\bar{\bar{\tau}}_g + \alpha_g \rho_g \vec{g} + K\left(\vec{v}_s - \vec{v}_g\right) \quad (4)$$

The equation for granular temperature:

$$\frac{3}{2}\left[\frac{\partial}{\partial t}\left(\alpha_s \rho_s \Theta_s\right) + \nabla.\left(\alpha_s \rho_s \vec{v}_s \Theta_s\right)\right] = \left(-p_s \bar{\bar{I}} + \bar{\bar{\tau}}_g\right) : \nabla.\vec{v}_s + \nabla.\left(K_{\Theta s} \nabla \Theta_s\right) - \gamma_{\Theta s} + \varphi_{gs} \quad (5)$$

Gas and solid phase stress tensor equations:

$$\bar{\bar{\tau}}_g = \alpha_g \mu_g \left(\nabla \vec{v}_g + \nabla \vec{v}_g^T\right) - \frac{3}{2}\alpha_g \mu_g \left(\nabla \vec{v}_g\right) I \quad (6)$$

$$\bar{\bar{\tau}}_s = \alpha_s \mu_s \left(\nabla \vec{v}_s + \nabla \vec{v}_s^T\right) - \alpha_s \left(\lambda_s - \frac{2}{3}\mu_s\right)\left(\nabla \vec{v}_g\right) I \quad (7)$$

Where; μ_s is the solid shear viscosity and λ_s is the solid bulk viscosity.

Solid phase properties are determined as a function of granular temperature according to the following equations:

$$p_s = \alpha_s \rho_s \Theta_s + 2\rho_s (1 - e_{ss}) \alpha_s^2 g_{o,ss} \Theta_s \quad (8)$$

$$\mu_s = \frac{4}{5}\alpha_s \rho_s d_s g_{o,ss}(1 + e_{ss})\left(\frac{\Theta_s}{\pi}\right)^{1/2} + \frac{\alpha_s d_s \rho_s \sqrt{\Theta_s \pi}}{6(3 - e_{ss})}\left[1 + \frac{2}{5}(1 + e_{ss})(3e_{ss} - 1)\alpha_s g_{o,ss}\right] \quad (9)$$

$$\lambda_s = \frac{4}{3}\alpha_s \rho_s d_s g_{o,ss}(1 + e_{ss})\left(\frac{\Theta_s}{\pi}\right)^{1/2} \quad (10)$$

Here, e_{ss} is the coefficient of restitution and it is given as an input parameter. The radial distribution function $g_{o,ss}$ is calculated as:

$$g_{o,ss} = \left[1 - \left(\alpha_s / \alpha_{s,max}\right)^{1/3}\right]^{-1} \quad (11)$$

Equation for drag coefficient:

$$K_{gs} = 150\frac{\alpha_s^2\mu_g}{\alpha_g d_s^2} + 1.75\frac{\alpha_s\rho_g|\bar{v}_s-\bar{v}_g|}{d_s} \quad \text{for } \alpha_g \le 0.8 \tag{12}$$

$$K_{gs} = \frac{3}{4}C_D\frac{\alpha_s\rho_g|\bar{v}_s-\bar{v}_g|}{d_s}\alpha_g^{-2.65} \quad \text{for } \alpha_g > 0.8 \tag{13}$$

Where,

$$C_D = \begin{cases}\frac{24}{Re_s}[1+0.15(Re_s)^{0.687}] & \text{for } Re_s \le 1000 \\ 0.44 & \text{for } Re_s > 1000\end{cases} \tag{14}$$

$$Re_s = \frac{\alpha_g\rho_g d_s|\bar{v}_s-\bar{v}_g|}{\mu_g} \tag{15}$$

3.3 Initial and Boundary Conditions

Initially, coal and biomass particles are patched upto a height as per the experimental condition. Air is introduced with a uniform velocity from the bottom inlet. No-slip boundary condition is applied for the gas phase at the wall. Jonson and Jackson (1987) slip boundary condition is applied for the solid phase at the wall as given below:

$$v_{s,w} = -A\frac{\partial v_{s,w}}{\partial n} \tag{16}$$

Where the slip coefficient A is expressed in terms of a specularity coefficient ϕ, as given below:

$$A = \frac{6\mu_s\alpha_{s,max}}{\sqrt{3}\pi\phi\rho_s\varepsilon_s g_{o,ss}\sqrt{\Theta}} \tag{17}$$

The value of specularity coefficient $\phi = 0.6$ is used for all the simulations (Loha *et al.* 2013). Atmospheric pressure boundary condition is used at the outlet.

3.4. Solution Procedure

Commercial CFD package ANSYS FLUENT is used for solving the above equations. An extension of SIMPLE algorithm (Patankar, 1980) for multiphase flow called Phase Couple SIMPLE algorithm is used for the Pressure-Velocity coupling. 2nd Order Implicit scheme is used for unsteady formulation and QUICK algorithm is used for discretization of convective terms. Each simulation is run for 30 s and the time-averaging is done between 5 s to 30 s. A small time step of $1x10^{-4}$ s is used to avoid the instability.

4. RESULTS AND DISCUSSION

4.1 Grid independence Study

In order to check the grid dependency of the numerical solution, simulations are run with three different grid sizes for a mixture of 90% coal and 10% biomass and results are compared. Three different grid sizes are; (a) a coarse grid (50 x 10) where cells are bigger than 10 times the particle diameter, (b) a medium grid (66 x 13) where cells are approximately 10 times the particle diameter and (c) a fine grid (80 x 16) where cells are smaller than 10 times the particle diameter. The time-average particle volume fraction distributions along the height of the reactor are plotted for three different grid sizes in Fig. 3. It is illustrated that there is no significant difference in the time-average particle volume fraction distribution for three different grid sizes. The particle volume fraction inside the bed and the bed height prediction by the coarse grid and the medium grid are identical. Whereas, the fine grid predicts little lower particle volume fraction inside the bed and little higher bed height. However, the maximum difference in particle concentration between fine grid and coarse grid is within 2 %. To get further inside, the pressure drop across the bed obtain from simulations by three grid sizes are compared with the experimental pressure drop as shown in Table 1. It is observed that the pressure drop prediction from the medium grid (66 x 13) simulation is nearest to the experimental data and farthest from the fine grid (80 x 16) simulation. In bubbling fluidized bed, other researchers (Gelderbloom *et al.* 2003; Jung *et al.* 2006) also reported that the bubble size computed with a grid size of about 10 times the particle diameter agreed well with their experimental results which is in line with our observation here. Therefore, all other simulations are run with the medium grid side (66 x 13).where cells sizes are approximately 10 times the particle diameter.

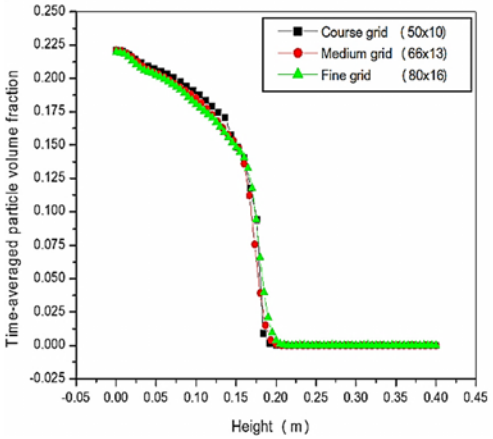

Fig. 3. Time-average particle volume fraction distribution for three different grid sizes of (50x10), (66x13) and (80x16).

Table 1 Comparison of pressure drop across the bed with three different grid sizes

S. No.	Grid Size	Pressure drop across the bed (Pa)
1	Coarse grid (50 x 10)	699
2	Medium grid (66 x 13)	686
3	Fine grid (80 x 16)	708
4	Experiment	665

4.2 Comparison of Bed Pressure Drops for Different Coal and Biomass Weight Percentages

Fig. 4 shows the pressure drop across the bed for different coal and biomass weight percentages

(100:0, 95:5, 90:10, 80:20, 70:30 and 50:50) obtain from simulations. The available experimental values of pressure drop are also plotted for comparison. Close agreement is observed between simulation and experimental pressure drop values. It is further observed that both the pressure drop obtain from simulations and experiments show similar trend of decrease with increase in biomass percentage. The decrease in pressure drop with the increase in biomass percentage could be explained due to the fact that biomass has less density compared to coal. As the biomass percentage increases in the mixture, the overall mass of the mixture decreases which requires less pressure force for fluidization.

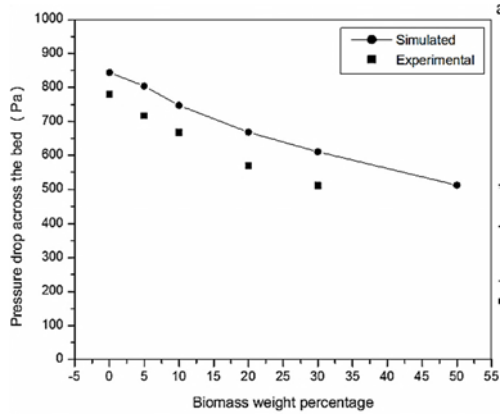

Fig. 4. Comparison of pressure drop for different coal and biomass weight percentages.

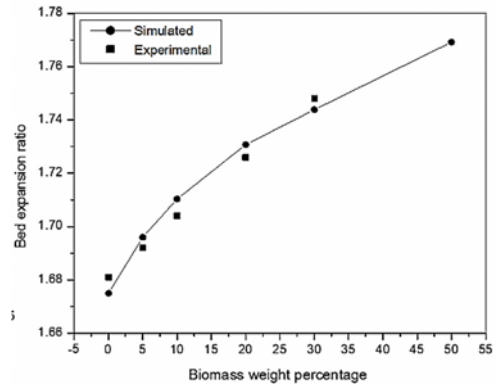

Fig. 5. Comparison of bed expansion ratio for different coal and biomass weight percentages.

4.3 Comparison of Bed Expansion Ratios for Different Coal and Biomass Weight Percentages

The bed expansion ratio is calculated by dividing the expanded bed height to the initial bed height for simulation and experiment in both the cases. Bed expansion ratios for different coal and biomass weight percentages obtain from simulations and experiments are plotted in Fig. 5. It is observed that the bed expansion ratio increases with increase in the biomass percentage for both the cases in simulation as well as in experiment. Bed expansion ratios obtain from simulations matching very well with the experimental values available. But, it is observed that the experimental bed expansion ratios obtain in the range (0% biomass to 30% biomass) increases almost linearly with increase in biomass percentages. Whereas, bed expansion ratios obtain from simulations (0% biomass to 50% biomass) increases non-linearly with the increase in biomass percentage. The flow ability of bulk solids largely depends upon their size and shape. In the present simulation, coal and biomass particles are assumed as spherical and having a mean particle diameter for each. Whereas, in practical coal and biomass particles are irregular in shape and they have different particle size distributions. These may be the reasons for showing different trends of bed expansion ratios in experiment and simulation.

4.4 Particle Volume Fraction and Velocity Distributions Inside the Computational Domain

Figure 6 shows the time-average particle volume fraction and velocity distributions for 100% coal, 95% coal and 5% biomass, 90% coal and 10% biomass, 80% coal and 20% biomass, 70% coal and 30% biomass and 50% coal and 50% biomass. The simulation results indicate that the region having maximum volume fraction of coal is initially at some height from bottom of the bed and it shifts downward as biomass percentage increases. It is observed that there is no significant change in particle volume fraction distribution upto 10% biomass weight percentage. But, further increase in biomass percentage changes the pattern of particle volume fraction distribution. Although, the value of maximum volume fraction of coal is not changing significantly but the location of maximum volume fraction is changing while the biomass percentage is increasing from 10% to 20%. An increase in bed height of biomass particles compare to coal particles is observed for biomass percentage of 20% and above.

The difference between the bed height of biomass particles and coal particles increases with increasing the biomass percentage from 20% to 50%. It is illustrated from the time-average particle velocity distribution that the particles are going up through the central region and coming down in the near wall region for all the cases. A nearly symmetric particle velocity distribution around the central axis is observed where two vortexes are formed one in each side of the axis in the upper portion of the bed. This type of velocity distribution indicates good mixing of particles within the bed.

4.5 Effect of Biomass Weight Percentage on Lateral Particle Velocity Distribution

Figure 7 shows the axial velocity distribution of coal and biomass particles in the lateral direction for varying weight percentages. Particle velocity distributions are plotted at two different bed heights of H=0.10 m and H=0.15m from the bottom of the reactor. Velocity distributions for different weight percentages are shown in the same graph with different colours and symbols and corresponding weight percentages are mentioned in the legend.

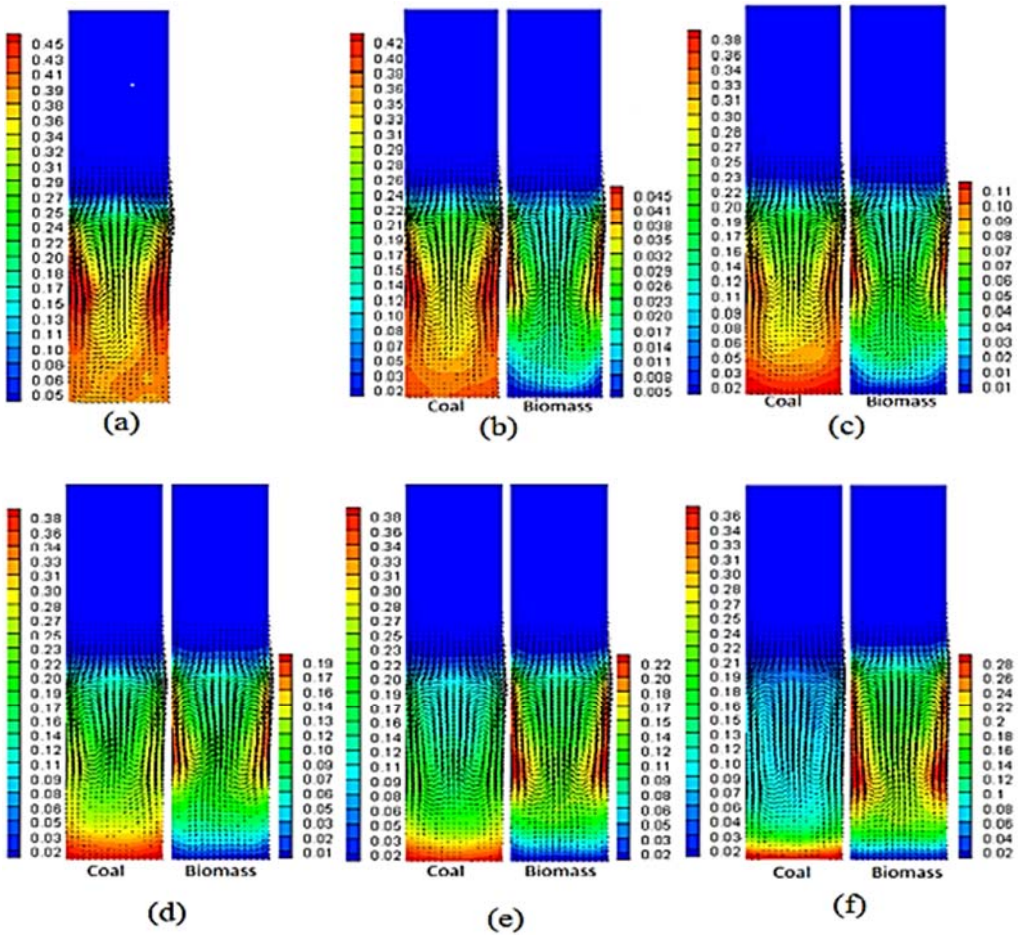

Fig. 6. Time-average particle volume fraction and velocity distribution; (a) 100% coal, (b) 95% coal and 5% biomass, (c) 90% coal and 10% biomass, (d) 80% coal and 20% biomass, (e) 70% coal and 30% biomass, (f) 50% coal and 50% biomass.

igure shows apparently symmetric distribution of velocities about the central axis. However, they are not exactly symmetric. The upward velocity of particles in the central region decreases due to increase in biomass percentage upto 10% and then increases with increasing biomass percentage upto 50%. However, in the near wall region, the downward velocity of particles increases continuously with the increase in biomass percentage. The change in particle velocity profile with the change in biomass percentage is significant at H=0.10 m compared to at H=0.15 due to the presence of more particles at the lower bed height.

Effect of Biomass Weight Percentage on Lateral Particle Volume Fraction Distribution

Figure 8 shows the particle volume fraction distribution in the lateral direction at two different bed heights of H=0.10 m and

H=0.15 m from the bottom of the reactor. It is observed that the particle volume fraction near the wall is higher and lower in central region for both coal and biomass which indicates more bubble formation in the central region compare to the near wall region. It is further observed that the particle volume fraction of coal decreases with the decrease in coal weight percentage [Fig.8a and Fig.8c] and particle volume fraction of biomass decreases with decrease in biomass weight percentage [Fig.8b and Fig.8d]. It is important to notice here that there is a significant change in particle volume fraction distribution for both coal and biomass while biomass weight percentage changes from 10% to 20%.

5. CONCLUSIONS

Hydrodynamics of coal and biomass mixture is studied numerically using Eulerian-Eulerian CFD model. Different weight percentage of coal and biomass (100:0, 95:5, 90:10, 80:20, 70:30 and 50:50) are used and their effects on thehydrodynamic behaviour are studied in detail. Some of the numerical results are also compared with the experimental data for validation. The study shows that with the increase in biomass weight percentage in the mixture, the pressure drop across the bed decreases. It is further observed that in the central region the particle volume fraction is low and particle velocity is high compared to the near wall region which indicates more bubble

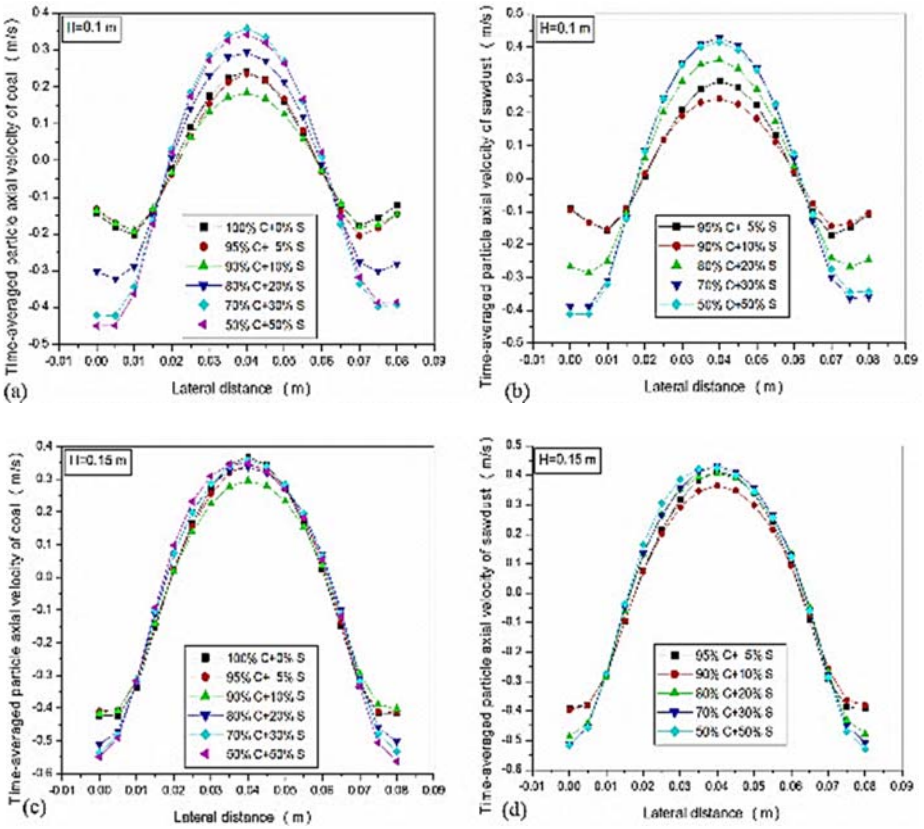

Fig. 7. Time-average axial velocity distribution of coal and biomass in the lateral direction at two different bed heights; (a) coal at H=0.10 m, (b) biomass at H=0.10 m, (c) coal at H=0.15m and (d) biomass at H=0.15 m.

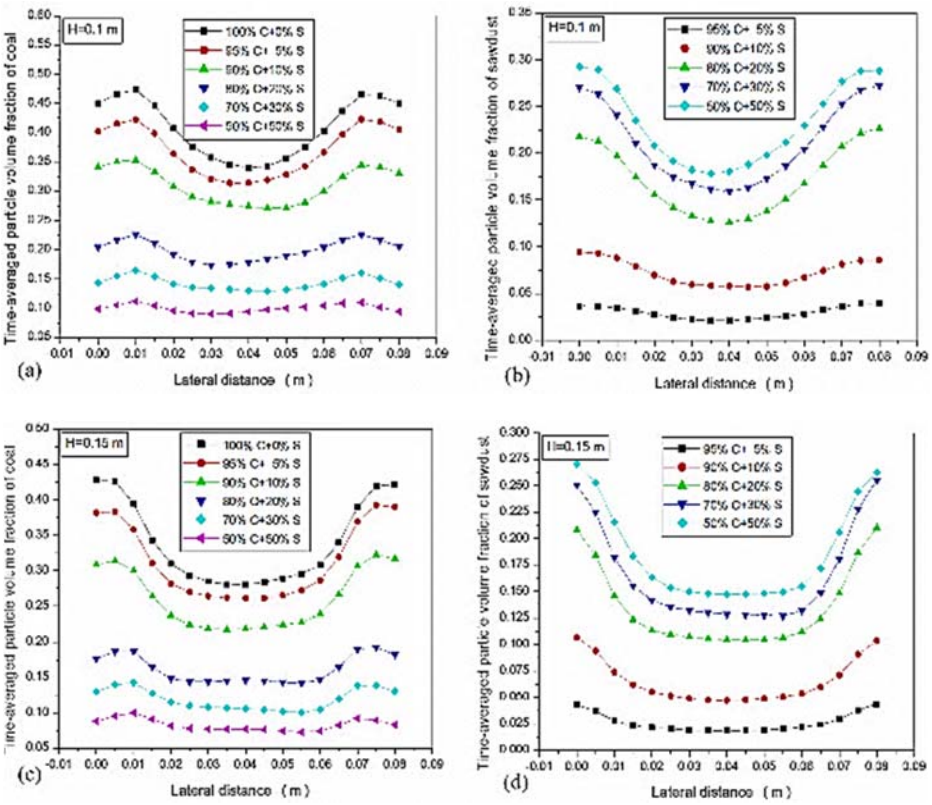

Fig. 8. Time-average particle volume fraction distribution of coal and biomass in the lateral direction at two different bed heights; (a) coal at H=0.10 m, (b) biomass at H=0.10 m, (c) coal at H=0.15m and (d) biomass at H=0.15 m.

formation in the central region compared to the near wall region. The particle volume fraction inside the bed as well as the lateral particle volume fraction distribution both show a significant change while biomass weight percentage increases from 10% to 20% in the mixture.

ACKNOWLEDGEMENT

The authors express their gratitude to the Director, CSIR-CMERI & the Director NIT Patna for their kind support to carry out the research work.

REFERENCES

Armstrong, L. M., K. H. Luo and S. Gu (2010). Two-dimensional and three-dimensional computational studies of hydrodynamics in the transition from bubbling to circulating fluidised bed. *Chemical Engineering Journal 160*, 239–248.

Bai, W., N. K. G. Keller, T. J. Heindel and R. O. Fox (2013). Numerical study of mixing and segregation in a biomass fluidized bed, *Powder Technology 237*, 355–366.

Buragohani, B., P. Mahanta and V.S. Moholkar (2010). Biomass gasification for decentralized power generation: the Indian perspective. *Renewable and Sustainable Energy Reviews 14*, 73–92.

Busciglio, A., G. Vella and G. Micale (2012). On the bubbling dynamics of binary mixtures of powders in 2D gas-solid fluidized beds, *Powder Technology 231*, 21–34.

Chen, H., D. Yang and J. Cheng (2015). Hydrodynamics of gas solids in a bubbling fluidized bed with binary Particles. *Procedia Engineering 102*, 799 – 803.

Cloete, S., S. T. Johansen and S. Amini (2013). Investigation into the effect of simulating a 3D cylindrical fluidized bed reactor on a 2D plane. *Powder Technology 239*, 21–35.

Deen, N. G., M. Van Sint Annaland and J. A. M. Kuipers (2006). Detailed computational and experimental fluid dynamics of fluidized beds. *Applied Mathematical Modelling 30*, 1456□1471.

Gao, J., J. Chang, C. Lu and C. Xu (2008). Experimental and computational studies on flow behavior of gas–solid fluidized bed with disparately sized binary particles. *Particuology 6*, 59–71.

Gelderbloom, S. J., D. Gidaspow and R.W. Lyczkowski (2003). CFD simulations of bubbling/collapsing fluidized beds for three Geldart groups. *AIChE Journal 49*, 844–858.

Johnson, P. C. and R. Jackson (1987). Frictional–collisional constitutive relations for granular materials with application to plane shearing. *Journal of Fluid Mechanics 176*, 67–93.

Jung, J., D. Gidaspow and I. K. Gamwo (2006). Bubble computation, granular tem-peratures, and Reynolds stresses. *Chemical Engineering Communications 193*, 946–975.

Loha, C., H. Chattopadhyay and P. K. Chatterjee (2013). Euler-Euler CFD modeling of fluidized bed: Influence of specularity coefficient on hydrodynamic behavior. *Particuology 11*, 673–680.

Loha, C., H. Chattopadhyay and P. K. Chatterjee (2012). Assessment of drag models in simulating bubbling fluidized bed hydrodynamics. *Chemical Engineering Science 75*, 400–407.

Patankar, S.V. (1980). *Numerical heat transfer and fluid flow*, New York: Hemisphere Publishing Corporation.

Sau, D. C. and K. C. Biswal (2011). Computational fluid dynamics and experimental study of the hydrodynamics of a gas–solid tapered fluidized bed. *Applied Mathematical Modelling 35*, 2265□2278.

Sharma, A., S. Wang, V. Pareek, H. Yang and D. Zhang, (2014). CFD modeling of mixing/segregation behavior of biomass and biochar particles in a bubbling fluidized bed. *Chemical Engineering Science 106*, 264–274.

Verma, M., C. Loha, A. N. Sinha and P. K. Chatterjee (2017). Drying of biomass for utilising in co-firing with coal and its impact on environment□A review. *Renewable and Sustainable Energy Reviews 71*, 732□741.

Wang, X. Y., F. Jiang, X. Xu, B. G. Fan, J. Lei and Y. H. Xiao (2010). Experiment and CFD simulation of gas–solid flow in the riser of dense fluidized bed at high gas velocity. *Powder Technology 199*, 203–212.

Witta, P. J., J. H. Perrya and M. P. Schwarz (1998). A numerical model for predicting bubble formation in a 3D fluidized bed. *Applied Mathematical Modelling 22*, 1171□1080.

Yu, L., J. Lu, X. Zhang and S. Zhang (2007). Numerical simulation of the bubbling fluidized bed coal gasification by the kinetic theory of granular flow (KTGF). *Fuel 86*, 722–734.

Zhang, K., B. Yu, J. Chang, G. Wu, T. Wang and D. Wen (2012). Hydrodynamics of a fluidized bed co-combustor for tobacco waste and coal. *Bioresource Technology 119*, 339–348.

Zhu, H., J. Zhu, G. Li and F. Li, (2008). Detailed measurements of flow structure inside a dense gas–solids fluidized bed. *Powder Technology 180*, 339–349.

Zimmermann, S. and F. Taghipour (2005). CFD modeling of the hydrodynamics and reaction kinetics of FCC fluidized-bed reactors. *Ind. Eng. Chem. Res. 44*, 9818–9827.